

Photonic Bound State in the Continuum for Strong Light-matter Interaction

Chang-Ling Zou, Jin-Ming Cui, Fang-Wen Sun,* Xiao Xiong, Xu-Bo Zou, Zheng-Fu Han, and Guang-Can Guo
 Key Lab of Quantum Information, University of Science and Technology of China, Hefei 230026

The photonic bound state in the continuum (BIC) is discovered in a hybrid photonic circuit with low refractive index waveguide on a high refractive index thin membrane, where the optical dissipation is forbidden because of the destructive interference of different leakage channels. Based on the photonic BIC, the low mode area in a hybrid waveguide and high quality factor in a microresonator can be applied to enhance the light-matter interaction. Taking the fabrication-friendly polymer structure on diamond membrane as an example, those excellent optical performances can exist in a wide range of structure parameters with large fabrication tolerance and induce the strong coupling between photon and nitrogen-vacancy center in the diamond for scalable quantum information processors and networks. Such a fabrication-friendly structure with photonic BIC is also very promising in laser, nonlinear optical and quantum optical applications.

PACS numbers: 42.55.Sa, 05.45.Mt, 42.25.-p, 42.60.Da

Introduction.- Great progresses have been achieved recently in the photonic integrated circuits (PIC) for classic and quantum information processes [1, 2]. Efforts have been dedicated to exploit new materials, such as materials with excellent nonlinear optical properties [3–6] and solid quantum emitters [7, 8], for better optical performances and functionality. And a range of new physical phenomena has been studied in PIC and applied to develop new components, including the photonic Aharonov-Bohm effect [9] and topological insulator [10, 11]. In PIC, photons are processed by the basic components composed of waveguide and resonator structures, where high refractive index (RI) contrast to environment is essential. It has been long known that the light in low RI contrast structure will leak through coupling to continuum modes in substrate. This can be intuitively explained by quantum physics that the wave cannot be localized upon a potential well. Thus, the materials for PICs are restricted to high RI. However, fabrication difficulties are often encountered for some high RI materials, such as the diamond whose optical performances suffer from the surface scattering caused by sidewall roughness [12, 13].

It is instructive to consider the low RI contrast PIC. Actually, the bound states do exist upon potential well. This intriguing phenomenon, the so-called bound state in the continuum (BIC), was first proved by Von Neumann and Wigner in 1929 [14], and has been extensively studied recently in electronic and photonic structures [15–19]. In this Letter, we propose a novel photonic waveguide based on the BIC, which is made by low RI material on a high RI substrate, without specially engineered potential distribution [19] or multiple waveguides by the virtue of symmetry [18]. In such a hybrid waveguide, optical dissipating is forbidden because of the destructive interference of different dissipation channels under certain geometric parameters. Remarkably, the BIC is also demonstrated in the rotating-symmetry microring structure, allowing ultrahigh quality factor resonances. Therefore, our study brings the BIC from the basic scientific interest of funda-

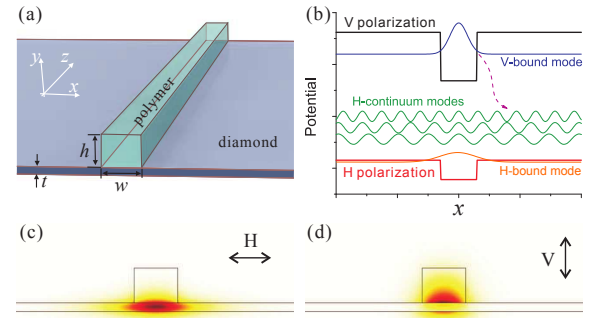


FIG. 1: (color online) (a) The hybrid photonic BIC structure with polymer waveguide on a thin diamond membrane. (b) The effective potential for modes. (c) and (d) Field distributions of Horizontal or Vertical polarized modes bounded to the waveguide, with polymer waveguide height $h = 400\text{nm}$, width $w = 500\text{nm}$, and membrane thickness $t = 100\text{nm}$.

mental quantum physics to practical applications, permitting a new kind of PIC. In this work, we take the diamond as an example, for the reason that photonic structure is very demanded to enhance the emission and collection of zero-phonon line (ZPL) of nitrogen-vacancy center (NVC) in diamond, then to improve the fidelity in quantum control [20, 21] and resolution in magnetic and biologic sensing [22, 23] with NVC. By combining with the NVCs and the fabrication-friendly polymer photonic structures on a diamond membrane, strong light-matter interaction is promising. The BIC based diamond chip provides an excellent platform for integrated quantum networks [24].

Bound State in the Continuum.- The light propagating in waveguide along z -axis with slow-varying approximation can be described by the Schrödinger equation

$$i2\beta\partial_z\psi(\mathbf{r}) = [\nabla^2 - U(\mathbf{r})]\psi(\mathbf{r}), \quad (1)$$

by replacing the time t by z . Here, $\psi(\mathbf{r})e^{i\beta z - i\omega t}$ is the scalar wave function, ω and β are respectively the

light frequency and propagation constant. The potential $U(\mathbf{r}) = \beta^2 - n^2(\mathbf{r})k^2$, with $n(\mathbf{r})$ is the dielectric RI and $k = 2\pi/\lambda$ is the vacuum wavenumber. Usually, waveguide structures are composed of high RI waveguides in low RI environment, where the guiding modes satisfy $U(\mathbf{r}) > 0$ in environment and the modes are well confined with only evanescent field outside. However, in the case of low RI waveguide in high RI environment, the mode energy is higher than the potential of environment as $U(\mathbf{r}) < 0$. The guiding mode coupling to continuum modes will lead to significant leaking loss.

To construct PICs beyond the limitation of high RI contrast, we consider the hybrid structure consisting of polymer waveguide on an air-suspended diamond membrane as depicted in Fig. 1(a). In this film-like substrate, wavefunctions are confined along y -direction, and the engineered continuum is reduced to be one dimensional (along x). Under the two-dimensional approximation by treating the regions with and without polymer both as film waveguides separately, the Schrödinger equation reduced to one-dimension as [25]

$$i\beta\partial_z\psi(x, z) = [\partial_x^2 - U(x)]\psi(x, z). \quad (2)$$

Here, $n(x)$ is replaced by the effective 2D RI. In the following, we focus on the working wavelength $\lambda = 637\text{nm}$ (ZPL of NVCs), with RIs of the polymer and diamond are $n_p = 1.49$ and $n_d = 2.41$, respectively. The effective RIs of the region with and without polymer for the Horizontal (Vertical) polarization are $n_{1,H(V)} = 1.879(1.536)$ and $n_{2,H(V)} = 1.820(1.171)$, which are obtained as the effective mode indices ($n_{eff} = \beta/k$) of fundamental propagation modes of the film waveguide. As shown in Fig. 1(b), the external polymer waveguide induces a potential well which gives rise to bound modes. Figures 1(c) and 1(d) are the numerically solved fundamental bound modes with different polarization. Since the depth of the potential well for horizontal-polarized bound mode (HBM) is much lower than that for vertical-polarized bound mode (VBM), the HBM is weakly confined in the membrane and widely distributed along x -direction, while the VBM is strongly confined laterally. This result suggests that very large loss of HBM for bending waveguides in practical applications. Therefore, we restrict the study to VBM in the following.

It is intuitively obvious that the VBM can dissipate through coupling to infinite horizontal-polarized continuum modes (HCM) above the potential barrier, due to the energy of VBM is much higher than the potential barrier of HBM [Fig. 1(b)]. The Hamiltonian for the VBM in continuum modes can be written as ($\hbar c = 1$)

$$H = \beta_b b^\dagger b + \sum_m \beta_m c_m^\dagger c_m + \sum_m (g_m c_m^\dagger b + h.c.), \quad (3)$$

with b and c_m are respectively annihilation operators of the VBM and m -th HCM, β_b and β_m are the corresponding propagation constants, g_m is the coupling strength.

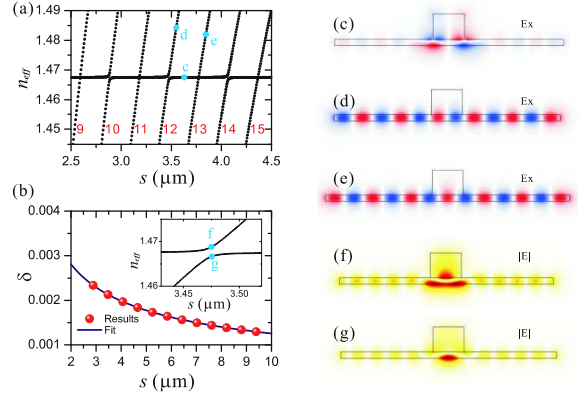


FIG. 2: (color online) (a) The effective mode indices of VBM and HSMs with varying slab width s . (b) The minimal effective mode index differences at anticrossing. Inset: the anti-crossing for $m = 12$. (c)-(g) Field distributions of s denoted in (a) and (b), with same h , w and t in Fig.1.

BIC in Hybrid Waveguide.- We firstly study the coupling between VBM and HCMs of a slab with finite width s . In this case, HCMs are discrete under the quantization condition $k_x s \approx 2\pi m$, with the wave-vector along x -direction $k_x = \sqrt{n_{2,H}^2 - n_m^2} k$. The integer m is the order of HCM and $n_m = \beta_m/k$ is the effective mode index. Figure 2(a) shows the numerically solved effective mode indices of eigenmodes in the hybrid waveguide, where $n_m \approx \sqrt{n_{2,H}^2 - (2\pi m/k s)^2}$ changes with s while the effective mode index of VBM $n_b = \beta_b/k$ is constant. When VBM and HSMs are near resonance ($n_m \approx n_b$), there are two different behaviors in the trajectories of the mode index against s : crossing when m is odd and anti-crossing when m is even. To interpret these results, the profiles of horizontal component of electric field (E_x) for VBM and HSMs are plotted in Fig. 2(c)-2(e). Although the electric field of VBM is quasi-V-polarized, its E_x is nonzero at corners due to diffraction [Fig. 2(c)]. The parity of E_x of VBM is odd while parity of m -th HSM is determined by m [Figs. 2(d) and 2(e)]. When m is odd, the VBM is orthogonal with m -th HSM and their mode index trajectories cross each other without interplay. However, for even m , the overlap between wavefunctions of VBM (φ_b) and m -th HSM (φ_m) will induce coupling. Due to the interaction, the eigenmodes of this hybrid waveguide are hybridization of VBM and HSMs, showing an effective index difference between the eigenmodes are $\delta = \sqrt{4g_m^2 + \Delta^2}/k$, with $\Delta = (n_m - n_b)k$ is the detuning. It means that nonzero g_m leads to the anti-crossing that δ is always greater than 0. As an example, a detailed illustration of anti-crossing between VBM and 12-th HSM is shown in the inset of Fig. 2(b). When the two modes are on-resonance ($n_{12} = n_b$), the splitting between two eigenmode branches reaches the minimum ($\delta = 2g_{12}/k$), with hybrid eigenmodes shown in Figs. 2(f)

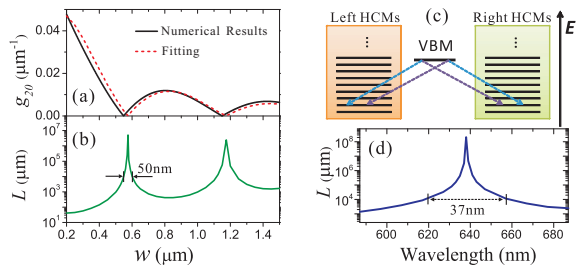


FIG. 3: (color online) (a) The coupling strength g_{20} against waveguide width w . The solid line is the numerical simulation result, and the dashed line is the analytical result. (b) The propagation length of the bound waveguide modes for $s = \infty$ against the waveguide width with $\lambda = 637\text{nm}$. (c) The schematic illustration of the BIC for the VBM coupled to the HCMs. (d) The calculated propagation length L of VBM for $s = \infty$ against wavelength, with $w = 575\text{nm}$.

and 2(g).

The coupling strength g_m depends on the normalized field overlap between VBM and HSM which is approximately proportional to $1/w\sqrt{s}$. As shown in Fig. 2(b), the minimums $\delta = 2g_m/k$ which are deduced from Figs. 2(a) are plotted and consistent with the fitting by $1/\sqrt{s}$. There are two channels for VBM dissipating to each continuum mode as diffracting at corners of waveguide. As a consequence, we have

$$g_m \approx \tilde{g}_m \times \frac{|1 + e^{ik_x w}|}{2w\sqrt{s}}, \quad (4)$$

which contains the interference of two channels with paths phase difference $k_x w \approx \sqrt{n_{2,H}^2 - n_m^2} kw$, and \tilde{g}_m is constant. This means that the dissipation of VBM can be totally frozen ($g_m = 0$) by carefully choosing geometry of polymer waveguide: when $\cos(k_x w) = -1$ is achieved, the dissipation cancels because of the destructive interference, leading to a photonic BIC. To confirm this conclusion, we calculate g_{20} as a function of w numerically from anti-crossings $g_m = \delta k/2$. As displayed in Fig. 3(a), the data are consistent with Eq. (4), showing oscillations and approaching zero at certain w .

Since there are infinite continuum modes when s goes infinite, the membrane serves as a reservoir and the dynamics of VBM is Markovian. Thus, the energy of VBM exponentially decays with propagation distance as $I(z) = I(0)e^{-z/L}$ with the decay length $L = \sqrt{n_{2,H}^2 - n_b^2}/2g_b^2 sn_b$ [26]. Here, g_b is the coupling strength between VBM and near resonance HSM ($n_m \approx n_b$), and $g_b^2 s \approx [\tilde{g}_m \cos(\frac{k_x w}{2})/w]^2$ is independent on s . Figures 3(b) and 3(d) show the dependence of L on w and wavelength. These results indicate that L can be larger than 1m, corresponding to the BIC that VBM is almost totally decoupled from the continuum modes.

BIC in Hybrid Microresonator.- Microresonator is another important component in PIC, which can trap light

and enhance the light-matter interaction. Figure 4(a) is a typical microring resonator coupled to a waveguide, whose geometry is characterized by the width of cross section (w_r) and exterior radius (R). Whispering gallery modes (WGMs) in such hybrid microring are solved numerically by an axis-symmetry model, with a perfect match layer applied to calculate the quality factor (Q) accurately. For the vertical-polarized WGMs, similar to the waveguide VBM, the bound modes will couple to the continuum modes inevitably, which will induce extra energy loss and limit the Q of WGMs. In such axis-symmetry structure, the WGMs couple to the horizontal-polarized cylindrical waves in membrane $J_q(nkr)e^{iq\phi}$, where $J_q(z)$ is Bessel function of order q [27]. However, since the mode profile of WGMs tends to outer corner [Fig. 4(b)], the two passages of dissipation (diffraction at two corners) are unbalanced. The loss of bound modes to continuum is proportional to $|J_q(nkR) - \xi J_q(nk(R - w_r))|$, where the factor $\xi < 1$ accounts for the asymmetric coupling strengths at two corners. In Figs. 4(d) and 4(e), the leaking loss and Q of WGMs with wavelength around 637nm is calculated against R . The prediction is consistent with numerical results. The oscillation of dissipation loss and Q is due to the standing-wave behavior of cylindrical Bessel wave in the radius direction. There are several peaks of Q greater than 10^6 in Fig. 4(e), indicating the existence of BIC, i.e. the two dissipation channels cancel each other for specific R s. It is worth noting that the horizontal-polarized WGMs are not found in our numerical simulations, due to their extremely low Q caused by very large bending loss of HBM.

Strong Coupling.- Utilizing the Purcell effect [28], the coherent ZPL emission of NVC embedded in diamond will be enhanced by interacting with bound photonic modes. For example, the effective mode area of hybrid waveguide is $A = 0.092\mu\text{m}^2$ for $w = 570\text{nm}$, corresponding to enhanced spontaneous emission with Purcell factor $F = 2.74$ and waveguide collection efficiency of ZPL $\zeta = F/(F + 1) = 0.73$. In addition to the enhanced emission and collection, the undesired phonon sidebands emission of NVC can be suppressed as the BIC can only exist around ZPL [Fig. 3(d)].

For the microring with $w_r = 0.57\mu\text{m}$ and $R = 6.6\mu\text{m}$, the Q of WGM is as high as 6.5×10^7 for BIC. The mode volume for NVC in diamond $V = 1.89\mu\text{m}^3$ can be approximated by πRA as the mode profile of WGMs at the cross section is close to that of waveguide. In such a high Q/V hybrid microresonator, the Purcell factor of ZPL can be as large as $F = \frac{3}{4\pi^2} \frac{Q}{V} \left(\frac{\lambda}{n_d}\right)^3 = 828$. The maximum coherence coupling strength between photon and zero-phonon transition of NVC is $G = \sqrt{\frac{\omega d^2}{2\hbar\epsilon V}} \times \eta \approx 242 \times 2\pi$ MHz, where d is the dipole momentum and $\eta = 0.05$ is the percentage of ZPL in the total emission of NVC. As the decay rate of NVC $\gamma \approx 13 \times 2\pi$ MHz, the strong coupling ($G > \gamma, \kappa$) can be achieved when the

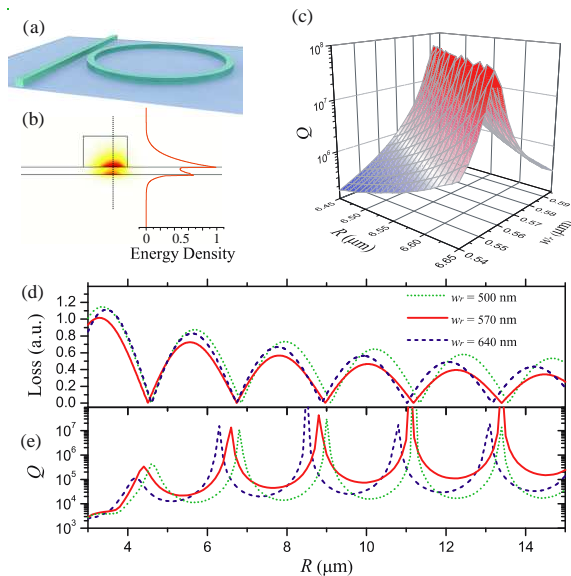


FIG. 4: (color online) (a) The schematic of the hybrid microring coupling to a hybrid waveguide. (b) The energy density distribution at the cross section of the hybrid microring. The solid curve is the field distribution along y -direction, as indicated by the dashed line. (c) The tolerance of the Q factor versus the R and microring width w_r . (d) and (e) The predicted loss and calculated Q factor of the microring against the radius R , with different microring width.

cavity dissipation rate $\kappa = \omega/2Q < G$, i.e. $Q > 10^6$. For practical experiment, the dependence of Q on the variance of R and w_r is studied in Fig. 4(c), showing good fabrication tolerance of BIC for strong coupling.

Discussion.- Based on the BIC, the proposed structure is feasible in experimental demonstration. The single crystal diamond membrane can be prepared by chemical methods [29, 30], and its surface roughness can be reduced to a few nanometers by mechanical polishing or phonon-assisted etching [31]. As for the polymer nanostructures, which possess very excellent optical properties and are compatible to other materials [32], they can be fabricated via mature nano-fabrication techniques, such as electron beam lithography, nano-imprint and direct laser writing. In addition, the BIC shows fabrication tolerance of wide range of parameters. For example, ensuring $L > 10$ mm, the fabrication tolerance of w and the wavelength bandwidth are about 50nm and 37nm, respectively. It worth noting that the diamond membrane is not necessary air-suspended, it can be supported on a low RI polymer or silica substrate.

Such a photonic BIC structure has shown nice optical performance for diamond-based photonic application and various applications with NVC. The general principles of BIC can also be extended to other low RI material on high RI substrate. For the photonic BIC waveguide with nonlinear optical materials, the optical mode with low effective area can be use to enhance the nonlinear in-

teraction, which is very promising in the chip-scale nonlinear optical application with novel optical phenomena. Lasers can be generated with the microring structure on the optical gain material with simple design. The photonic BIC also shows potentials in the application of new optical material without complicated nanophotonic fabrication.

Conclusion.- We have proposed and demonstrated the photonic BIC in low RI waveguide and microring structures on a high RI substrate. The BIC based PIC is feasible for the experiments. The circuit with polymer on diamond membrane with low loss BIC has fabrication tolerance of about 50nm. Strong coupling between ZPL transition of NVC and photon is possible, offering an excellent platform for future scalable quantum information processor and networks. Such a photonic BIC will also benefit many chip-scale optical applications in classic and quantum optics.

Acknowledgements This work was supported by the National Fundamental Research Program of China (No.2011CB921200), the Knowledge Innovation Project of Chinese Academy of Sciences (No.60921091), National Natural Science Foundation of China (No.11004184) and NCET.

* Electronic address: fwsun@ustc.edu.cn

- [1] B. E. Saleh and M. C. Teich, *Fundamentals of Photonics*, vol. 32 (Wiley-Interscience Hoboken, NJ, 2007).
- [2] J. L. O'Brien and J. V. Akira Furusawa, *Nat. Photon.* **3**, 687 (2009).
- [3] T. Peyronel, O. Firstenberg, Q.-Y. Liang, S. Hofferberth, A. V. Gorshkov, T. Pohl, M. D. Lukin, and V. Vuletic, *Nature* **488**, 57 (2012).
- [4] B. J. Eggleton, B. Luther-Davies, and K. Richardson, *Nat. Photon.* **5**, 141 (2011).
- [5] K. Kim, S.-H. Cho, and C.-W. Lee, *Nat. Photon.* **6**, 502 (2012).
- [6] R. S. Jacobsen, K. N. Andersen, P. I. Borel, J. Fage-Pedersen, L. H. Frandsen, O. Hansen, M. Kristensen, A. V. Lavrinenko, G. Moulin, H. Ou, et al., *Nature* **441**, 199 (2006).
- [7] G. Balasubramanian, P. Neumann, D. Twitchen, M. Markham, R. Kolesov, N. Mizuochi, J. Isoya, J. Achard, J. Beck, J. Tissler, et al., *Nat. Mater.* **8**, 383 (2009).
- [8] W. F. Koehl, B. B. Buckley, F. J. Heremans, G. Calusine, and D. D. Awschalom, *Nature* **479**, 84 (2011).
- [9] K. Fang, Z. Yu, and S. Fan, *Phys. Rev. Lett.* **108**, 153901 (2012).
- [10] A. B. Khanikaev, S. Hossein Mousavi, W.-K. Tse, M. Kargarian, A. H. MacDonald, and G. Shvets, *Nat. Mater.* **12**, 233 (2013).
- [11] M. C. Rechtsman, J. M. Zeuner, Y. Plotnik, Y. Lumer, S. Nolte, M. Segev, and A. Szameit, *Nature* **496**, 196 (2013).
- [12] A. Faraon, P. Barclay, C. Santori, K. Fu, and R. Beausoleil, *Nat. Photon.* **5**, 301 (2011).

- [13] B. Hausmann, B. Shields, Q. Quan, P. Maletinsky, M. McCutcheon, J. Choy, T. Babinec, A. Kubanek, A. Yacoby, M. Lukin, et al., *Nano Lett.* **12**, 1578 (2012).
- [14] J. von Neumann and E. Wigner, *Phys. Z.* **30**, 465 (1929).
- [15] F. Capasso, C. Sirtori, J. Faist, D. Sivco, S. Chu, and A. Cho, *Nature* **358**, 565 (1992).
- [16] D. Marinica, A. Borisov, and S. Shabanov, *Phys. Rev. Lett.* **100**, 183902 (2008).
- [17] S. Díaz-Tendero, A. Borisov, and J. Gauyacq, *Phys. Rev. Lett.* **102**, 166807 (2009).
- [18] Y. Plotnik, O. Peleg, F. Dreisow, M. Heinrich, S. Nolte, A. Szameit, and M. Segev, *Phys. Rev. Lett.* **107**, 183901 (2011).
- [19] M. Molina, A. Miroshnichenko, and Y. Kivshar, *Phys. Rev. Lett.* **108**, 070401 (2012).
- [20] T. Ladd, F. Jelezko, R. Laflamme, Y. Nakamura, C. Monroe, and J.L. O'Brien, *Nature* **464**, 45 (2010).
- [21] P. Maurer, G. Kucsko, C. Latta, L. Jiang, N. Yao, S. Bennett, F. Pastawski, D. Hunger, N. Chisholm, M. Markham, et al., *Science* **336**, 1283 (2012).
- [22] H. Mamin, M. Kim, M. Sherwood, C. Rettner, K. Ohno, D. Awschalom, and D. Rugar, *Science* **339**, 557 (2013).
- [23] G. Kucsko, P. Maurer, N. Yao, M. Kubo, H. Noh, P. Lo, H. Park, and M. Lukin, arXiv preprint arXiv:1304.1068 (2013).
- [24] I. Aharonovich, A. D. Greentree, and S. Prawer, *Nat. Photon.* **5**, 397 (2011).
- [25] A. Zaghlool and A. Abou-El-Fadl, in *Radio Science Conference, 1999. NRSC'99. Proceedings of the Sixteenth National* (IEEE, 1999), pp. B9–1.
- [26] C.-L. Zou, X.-D. Chen, X. Xiong, X.-B. Zou, Z.-F. Han, G.-C. Guo, and F.-W. Sun, preprint arXiv:1212.6136 (2013).
- [27] C.-L. Zou, F.-J. Shu, F.-W. Sun, Z.-J. Gong, Z.-F. Han, and G.-C. Guo, *Opt. Express* **21**, 9982 (2013).
- [28] E. M. Purcell, *Phys. Rev.* **69**, 681 (1946).
- [29] B. Fairchild, P. Olivero, S. Rubanov, A. Greentree, F. Waldermann, R. Taylor, I. Walmsley, J. Smith, S. Huntington, B. Gibson, et al., *Adv. Mater.* **20**, 4793 (2008).
- [30] I. Aharonovich, J. Lee, A. Magyar, B. Buckley, C. Yale, D. Awschalom, and E. Hu, *Adv. Mater.* **24**, OP54 (2012).
- [31] T. Yatsui, W. Nomura, M. Naruse, and M. Ohtsu, *J. Phys. D: Appl. Phys.* **45**, 475302 (2012).
- [32] C. Dong, F. Sun, C. Zou, X. Ren, G. Guo, and Z. Han, *Appl. Phys. Lett.* **96**, 061106 (2010).